HHS Public Access

Author manuscript

Nat Genet. Author manuscript; available in PMC 2016 August 01.

Published in final edited form as:

Nat Genet. 2016 February 24; 48(3): 265–272. doi:10.1038/ng.3502.

An oncogenic MYB feedback loop drives alternate cell fates in adenoid cystic carcinoma

Yotam Drier[1,2,3,4], **Matthew J. Cotton**[1,2,3,4], **Kaylyn E. Williamson**[1,2,3,4], **Shawn M. Gillespie**[1,2,3,4], **Russell J.H. Ryan**[1,2,3,4], **Michael J. Kluk**[5], **Christopher D. Carey**[5], **Scott J. Rodig**[5], **Lynette M Sholl**[5], **Amir H. Afrogheh**[1], **William C. Faquin**[1], **Lurdes Queimado**[6], **Jun Qi**[7], **Michael J. Wick**[8], **Adel K. El-Naggar**[9], **James E. Bradner**[3,7], **Christopher A. Moskaluk**[10], **Jon C. Aster**[5], **Birgit Knoechel**[1,3,11,12,13], and **Bradley E. Bernstein**[1,2,3,4,13]

[1]Department of Pathology, Massachusetts General Hospital and Harvard Medical School, Boston, Massachusetts, USA

[2]Center for Cancer Research, Massachusetts General Hospital, Boston, Massachusetts, USA

[3]Broad Institute of MIT and Harvard, Cambridge, Massachusetts, USA

[4]Howard Hughes Medical Institute, Chevy Chase, Maryland, USA

[5]Department of Pathology, Brigham and Women's Hospital and Harvard Medical School, Boston, Massachusetts, USA

[6]Department of Otorhinolaryngology, The University of Oklahoma Health Sciences Center, Oklahoma City, USA

[7]Department of Medical Oncology, Dana-Farber Cancer Institute, Boston, Massachusetts, USA

[8]South Texas Accelerated Research Therapeutics, START, San Antonio, Texas, USA

[9]Department of Pathology, The University of Texas MD Anderson Cancer Center, Houston, Texas, USA

[10]Department of Pathology, University of Virginia Health Sciences Center, Charlottesville, Virginia, USA

[11]Division of Hematology/Oncology, Boston Children's Hospital, Boston, Massachusetts, USA

Correspondence should be addressed to B.E.B. (; Email: Bernstein.Bradley@mgh.harvard.edu) and B.K. (; Email: birgit_knoechel@dfci.harvard.edu)

[13]These authors contributed equally to this work.

Accession codes

European Genome-phenome Archive (EGA), accession number EGAS00001001457.

Author Contributions

B.K. and Y.D. designed and performed experiments and analyzed the data. B.K. and B.E.B. designed the experimental strategy and supervised the study and analysis. Y.D. carried out computational analyses. Y.D., B.K. and B.E.B. wrote the manuscript. J.C.A, M.J.C., K.E.W., S.M.G., C.D.C., S.J.R., L.M.S., M.J.W. contributed to experiments and data analysis. A.H.A., R.J.R., M.J.K., W.C.F, L.Q., J.Q., J.E.B., C.A.M., A.K.E.-N., and J.E.B. provided reagents, contributed to analysis and gave conceptual advice. All authors discussed the results and implications and reviewed the manuscript.

Competing financial interests

J.E.B. is a scientific founder of Tensha Therapeutics, which has licensed drug-like derivatives of the JQ1 bromodomain inhibitor from the Dana-Farber Cancer Institute. The remaining authors declare no competing financial interests.

[12]Department of Pediatric Oncology, Dana-Farber Cancer Institute, Boston, Massachusetts, USA

Abstract

Translocation events are frequent in cancer and may create chimeric fusions or 'regulatory rearrangements' that drive oncogene overexpression. Here we identify super-enhancer translocations that drive overexpression of the oncogenic transcription factor *MYB* as a recurrent theme in adenoid cystic carcinoma (ACC). Whole-genome sequencing data and chromatin maps reveal distinct chromosomal rearrangements that juxtapose super-enhancers to the *MYB* locus. Chromosome conformation capture confirms that the translocated enhancers interact with the *MYB* promoter. Remarkably, MYB protein binds to the translocated enhancers, creating a positive feedback loop that sustains its expression. MYB also binds enhancers that drive different regulatory programs in alternate cell lineages in ACC, cooperating with TP63 in myoepithelial cells and a Notch program in luminal epithelial cells. Bromodomain inhibitors slow tumor growth in ACC primagraft models *in vivo*. Thus, our study identifies super-enhancer translocations that drive *MYB* expression and provides insight into downstream MYB functions in the alternate ACC lineages.

Introduction

Chromosomal rearrangements that create a chimeric fusion gene or drive oncogene overexpression are common in cancer. The discovery of the "Philadelphia chromosome" translocation in chronic myelogenous leukemia, which creates the *BCR-ABL* fusion gene, ushered in an era of targeted therapy with kinase inhibitors. Oncogenic rearrangements that juxtapose a strong enhancer near an oncogene, triggering its overexpression, are also frequent in leukemia and lymphoma[1–3]. Recently, a similar enhancer hijacking mechanism was described in medulloblastoma[4], wherein chromosomal translocations involving enhancers cause over-expression of *GFI1* or *GFI1B*, which function as transcriptional repressors of tumor suppressor genes. In other cases, translocation events drive the expression of an oncogene by replacing its promoter with a highly active promoter, as is the case for *TMPRSS2-ERG* fusions in prostate cancer[5].

Adenoid cystic carcinoma (ACC) is a malignant neoplasm that arises within the secretory glands, most commonly in the salivary glands of the head and neck. Though typically slow growing, these tumors are locally aggressive, with a tendency to spread along nerves. Perhaps most challenging clinically, ACC can recur loco-regionally or with distant metastases decades after primary tumor resection, requiring careful long-term surveillance of all patients. Due to the resistance of these tumors to chemotherapy and radiation therapy, non-resectable cases are usually fatal[6].

The *MYB-NFIB* translocation is a molecular hallmark that is present in a majority of ACC[7]. *MYB* is a master transcription factor (TF) involved in cellular differentiation and proliferation. It functions as an oncogene in a variety of cancers, including breast cancer, pancreatic cancer, and leukemia[8]. The *MYB-NFIB* translocation reportedly disrupts the *MYB* 3′UTR, which contains a microRNA (miRNA) regulatory site that down-regulates *MYB* expression[9]. However, *MYB* translocations that retain the 3′UTR are still associated

with high *MYB* expression, indicating the existence of additional mechanisms for *MYB* overexpression in ACC.

Here we identify the juxtaposition of super-enhancer regions to the *MYB* locus as the unifying feature of ACC translocations. Detailed genomic and epigenomic analyses of ACCs reveal alternate rearrangements that translocate super-enhancers in the *NFIB* and *TGFBR3* loci either upstream or downstream of the *MYB* gene. MYB protein binds these super-enhancers, which loop to the *MYB* promoter, thereby establishing a positive feedback loop that sustains expression of this master regulator. MYB also binds a larger repertoire of enhancers genome-wide, which appear to support alternate ACC expression signatures in the myoepithelial and luminal epithelial compartments of ACC. BET bromodomain inhibitors, which disrupt enhancer functions, slow tumor growth in ACC primagraft models *in vivo*. However, these inhibitors appear to be ineffective against high grade ACCs that harbor activating mutations in the Notch pathway. Thus, we identify a novel mechanism of transformation in which a regulatory element rearrangement creates a positive feedback loop between an oncogenic TF protein and its gene locus, with implications for diagnosis and therapeutic strategies in ACC.

Results

Novel *MYB* translocations in ACC

A diagnostic feature of ACC is a t(6:9) rearrangement that translocates *MYB* to the *NFIB* locus, and results in high *MYB* expression[9]. This translocation results in a fusion gene whose coding sequence is almost identical to *MYB*, but with an altered 3′UTR that lacks negative regulatory elements and leads to increased transcript stability[9]. Yet, while nearly all ACCs overexpress *MYB*, only about 30% carry an actual fusion transcript[10].

We therefore examined whole genome sequencing data for 18 ACCs, including 12 published primary ACCs[7,11] and 6 primary patient-derived xenografts (ACC primagrafts). Consistent with previous reports, we identified *MYB* translocations as the main recurrent event (13 out of 18 ACCs) in these tumors (Fig. 1a). We confirmed the presence of *MYB* rearrangements in four of these primagrafts by PCR. *MYB* rearrangements in the primagrafts were verified by FISH previously[12]. We also confirmed by PCR representative rearrangements involving other loci that were detected in the sequencing data (Supplementary Fig. 1, Supplementary Table 1). These results support the validity of rearrangements detected from whole genome sequencing data for these 18 ACCs. Finally, we identified MYB rearrangements in two additional tumors by targeted paired-end sequencing. This yielded a total of 15 (out of 20) ACCs with MYB rearrangements.

We identified canonical *NFIB-MYB* fusions with loss of the *MYB* 3′ UTR in 6 of the 20 tumors (30%; Fig. 1b, Table 1). An additional 6 tumors (30%) harbor an *NFIB-MYB* rearrangement but retain the *MYB* 3′UTR. We also identified novel translocations involving the *MYB* locus: two tumors harbored rearrangements between *MYB* and the *TGFBR3* locus, and one tumor harbored a rearrangement between *MYB* and the *RAD51B* locus. We used quantitative RT-PCR to confirm that all of these rearrangements are associated with high levels of *MYB* expression (Fig. 1c). Notably, several rearrangements occur at the 5′ end

of the *MYB* gene, which is inconsistent with production of any fusion protein (Fig. 2a). These findings indicate that neither fusion gene products nor 3′ UTR loss are unifying features of ACC rearrangements, and raise the alternate possibility that these translocations increase *MYB* expression through regulatory alterations.

Enhancer rearrangements act as drivers of *MYB* activation

We postulated that ACC translocations might reposition distal regulatory elements in proximity to *MYB*, thereby triggering its overexpression. We therefore mapped the chromatin landscapes of 13 ACCs, including 5 primary specimens and 8 primagrafts. We mapped histone H3 lysine 4 trimethylation (H3K4me3), a promoter-associated mark, and H3 lysine 27 acetylation (H3K27ac), a marker of active enhancers[13]. In a subset of samples, we also mapped the enhancer-associated BET bromodomain protein BRD4. Overall H3K27ac patterns were similar across primary ACCs and primagraft models, but distinct from an ACC cell line derived by viral transformation[14]. The ACC landscapes were distinct from other tumor types and non-malignant tissues (Supplementary Fig. 2). The conserved epigenomic landscapes between primary tumor and primagraft, together with the conserved histology[12], support the fidelity of the *in vivo* primagraft models.

We next examined the genomic loci that were translocated to *MYB* in the various tumors – specifically, the regions downstream of *NFIB*, *TGFBR3* and *RAD51B*. We found that all three regions contain large clusters of enhancers that are active in ACCs (Fig. 2c,e). Indeed, when we collated super-enhancers in ACCs based on expanse and signal intensity of H3K27ac[15] and BRD4 occupancy[16] we identified several super-enhancers in the rearranged portions of *NFIB* and *TGFRB3* (Fig. 2b,c,e; Supplementary Fig. 3). We also identified smaller enhancers downstream of *RAD51B*, which was rearranged in one ACC (Supplementary Fig. 4). Interestingly *NFIB, TGFBR3* and *RAD51B* are all highly expressed in normal salivary gland, suggesting these regions are indeed active before transformation (Supplementary Fig. 5). These findings suggest that the various rearrangements in ACC may act by repositioning potent regulatory elements close to *MYB*.

To test whether specific enhancers within the translocated super-enhancers might activate the *MYB* promoter, we examined their physical proximity using Chromosome Conformation Capture (3C). First, we examined an ACC with a translocation involving *MYB* and the *NFIB* locus. We examined 8 acetylated elements located between 13 and 750kb from the *MYB* promoter. We identified 4 elements that demonstrated a significant interaction with the *MYB* promoter (Fig. 2d). We also examined a second ACC with a *MYB-TGFBR3* translocation. In this case, 7 out of 9 tested H3K27ac peaks interacted with the *MYB* promoter (Fig. 2f). These data suggest that the translocations reposition super-enhancers that subsequently loop to the promoter and sustain high-level *MYB* expression.

Positive feedback MYB circuit

To examine potential downstream targets of *MYB* overexpression, we mapped MYB protein binding genome-wide in 3 ACC primagrafts using ChIP-Seq. MYB binding profiles were similar across the 3 ACC primagrafts and strongly enriched for the MYB motif in all samples (CAGTT, $p<10^{-759}$). MYB binding patterns differ from published datasets for other

human and mouse tissues[17,18], yet share a statistically significant overlap: 62% overlap with MYB-bound promoters in MCF7 ($p<10^{-6}$); 60% overlap with MYB targets in mouse myeloid progenitors ($p<10^{-51}$).

Notably, MYB binds to the enhancers in the *NFIB* and *TGFBR3* loci that are translocated to the *MYB* locus in ACC (Fig. 3a). When we ranked MYB bound enhancers per gene by binding signal, the translocated enhancers were near the top ranked genes (*NFIB,* #5 in ACCX5M1, and #17 in ACCX16; *TGFBR3,* #77 in ACCX2; see Methods, Fig. 3b). Moreover, in the respective rearranged tumors, these MYB-bound enhancers physically interact with the *MYB* gene promoter (Fig. 2d,f; Fig. 3a). Thus, MYB binding to translocated enhancer clusters may augment its own expression by activating transcription of the *MYB* gene (Fig. 3c). To test whether the translocated enhancers can drive transcription in a MYB-dependent manner, we cloned five 250 bp intervals from the *NFIB* and *TGFBR3* enhancers into a minimal promoter vector. We tested these reporter constructs in Jurkat cells, which express high levels of MYB protein at baseline[19]. We found that four of the five elements strongly induce reporter activity. Moreover, we found that the activity of two of these elements was diminished when we mutated their MYB motifs (Supplementary Fig. 6). These data support the enhancer identify and MYB responsiveness of sequence elements juxtaposed to the *MYB* locus by rearrangements. They are most consistent with a model in which positive feedback sustains *MYB* expression in this disease.

MYB-related regulatory programs in ACC

To infer potential downstream effects of *MYB* overexpression, we called 13,278 high confidence MYB binding sites (Methods, Supplementary Table 2). A majority of these sites coincides with distal regulatory elements (75%), while a minority coincides with promoters (Fig. 3d). MYB shows a strong preference for active elements as marked by H3K4me3 (promoters) or H3K27ac (enhancers). We predicted MYB target genes by assigning MYB-bound enhancers to nearby genes that are expressed in ACC[12] (Methods). These genes are expressed at relatively higher levels in the primagrafts, compared to all expressed genes, but are weakly expressed in normal salivary gland (Fig. 3e). We refer to these genes as *putative* MYB targets as they are probabilistic predictions based on binding profiles and expression patterns, whose further validation will require the development of faithful *in vitro* models for ACC.

Putative MYB targets in ACC are enriched for genes related to development, migration, cell signaling, cell cycle, transcription regulation and angiogenesis (REACTOME, Gene Ontology, MSigDB; FDR<1%, Supplementary Table 3). Specific examples include *MYC, BCL2, AURKA, CCND1, MET, FGFR2, IGF1R, MALAT1, CASC4* and *NENF*. We compared these expression patterns to normal salivary gland[20]. Out of 4853 highly expressed MYB bound genes in ACC, 50% are also highly expressed in normal salivary gland, 38% show low levels of expression and 12% are not expressed. Functional annotation of putative MYB targets that are also expressed in the normal counterpart revealed enrichment for genes involved in neurodevelopmental processes. In contrast, putative MYB targets that are uniquely expressed in ACC are enriched for cell cycle regulators, including *CDK6* and *GMNN* (Supplementary Table 2). Thus, MYB may engage two distinct

regulatory circuits in ACC, one that reinforces a pre-existing neurodevelopmental program in salivary epithelial cells and another that drives proliferation.

We next sought to identify other TFs or pathways that mediate or cooperate with MYB-driven regulatory programs in ACC. We scanned the high confidence MYB peaks collated above for enriched TF motifs. As expected, the top ranked motif corresponded to the MYB consensus. The second ranked motif is the TP53/TP63/TP73 consensus ($p<10^{-340}$). *TP63* was also identified as a putative MYB target (Supplementary Fig. 7). To directly test whether TP63 co-binds with MYB, we mapped binding of this TF by ChIP-seq. Remarkably, we found that 81% of TP63 binding sites in ACC are co-bound by MYB (Supplementary Fig. 8). We next collated putative target genes near the top ranked MYB binding sites, focusing on TFs and transcriptional regulators (Fig. 3f, Supplementary Table 4). This revealed activators such as *EN1*, recently identified as a biomarker for high grade ACC[21], the *ARID1A* chromatin remodeler, which is mutated in ACC[11], and *NOTCH1*. In addition to *NOTCH1,* the Notch activators, *JAG1* and *JAG2,* and the Notch transcriptional repressor *SPEN,* were identified among these highly ranked putative MYB targets. These data suggest that MYB, TP63 and NOTCH signaling may coordinately orchestrate the diverse expression programs in ACC.

Inter- and intra-tumoral epigenetic heterogeneity in ACC

ACC is notable for its biphenotypic differentiation with myoepithelial and (luminal) epithelial cells arranged in a ‘cribriform’ pattern. This histology is seen in low grade (grade 1 and 2) tumors, which constitute the majority of ACC cases. However, a smaller fraction of tumors have a ‘solid’ histology dominated by luminal epithelial cells, and are more aggressive (grade 3). Grade 3 tumors can originate from grade 2 tumors, but more commonly presented independently[22,23]. We therefore considered how MYB might promote these alternate cell fates in ACC.

We focused in particular on regulatory programs related to TP63 and Notch, which were both highlighted by our epigenomic analysis. We first examined the expression of these regulators in 19 grade 2 ACCs (Fig. 4a, Supplementary Fig. 9, Table 2). Immunohistochemistry (IHC) confirmed strong staining for TP63 – a marker of myoepithelial cells[24] – specifically in the myoepithelial compartments. TP63 was conspicuously absent from the luminal epithelial tumor cells, which stain positive for KIT. We also stained these tumors for ICN1, the active intracellular form of NOTCH1. ICN1 is expressed only in the luminal epithelial cells, and is exclusive with TP63 (Fig. 4b). This exclusivity is consistent with established antagonism between TP63 and NOTCH1 during development[25,26]. Thus, MYB appears to coordinate seemingly opposing regulatory programs in the distinct cellular compartments of ACC.

We next examined TP63 and NOTCH1 expression in eight grade 3 ACCs. These more aggressive specimens lack TP63 staining, consistent with loss of the myoepithelial component. Remarkably, they all show strong diffuse staining for ICN1. ACCs can harbor activating mutations in *NOTCH1* or loss of function mutations in the *RBPJ* repressor *SPEN*[7,11,27]. These mutations are present in 7 out of 9 grade 3 tumors, but none of the lower grade tumors examined (Supplementary Table 5). The other two grade 3 tumors display

NOTCH1 alterations that may also upregulate Notch signaling- ACC X11 has a tandem duplication 3′ of *NOTCH1*, in a region containing *NOTCH1* enhancers; ACC D1 has partial 5′ deletion of *NOTCH1*, similar to deletions we and others recently detected in breast cancer and T-ALL[27–29].

To gain further insight into the circuits that drive these respective regulatory programs, we compared enhancer patterning between low and high grade ACCs. First, we performed unsupervised clustering of putative active enhancers based on their H3K27ac patterns across 13 primagrafts and primary tumors (Supplementary Fig. 10). This analysis distinguished sets of enhancers preferential to either grade 2 or grade 3 tumors, which we then scanned for over-represented TF motifs (Fig. 3g). The TP63 motif was highly enriched in grade 2 specific enhancers, while the RBPJ/Notch motif was enriched in grade 3 specific enhancers. *TP63* exists in two main isoforms, TAp63, a transcriptional activator, and ΔNp63, which lacks the transactivation domain and exerts stem-like and oncogenic functions[30]. Only the oncogenic isoform ΔNp63 is transcribed in our ACC cohort (Supplementary Fig. 7), as is frequently the case in salivary tumors[31].

Thus, TP63 appears to be a mediator of the MYB regulatory program in the myoepithelial component of low grade ACCs. Conversely, Notch signaling is active in luminal epithelial components of low grade ACC. Its further activation by somatic Notch pathway gain-of-function mutations likely underlies the switch to solid histology and the aggressive clinical course of grade 3 tumors.

BET and Notch inhibitors target alternate ACC phenotypes

Our findings suggest that chromosomal rearrangements in ACC engage a positive feedback loop, in which MYB protein activates juxtaposed super-enhancers, which loop to the MYB gene and sustain its expression. BET bromodomain inhibitors have been shown to suppress MYB function in acute myeloid leukemia[32] and, more generally, may suppress super-enhancers with strong BRD4 occupancy[16]. This suggests that MYB target loci in ACC, which also have high BRD4 occupancy (Supplementary Fig. 11), may be sensitive to BET bromodomain inhibition. We specifically hypothesized that grade 2 tumors would be particularly sensitive to bromodomain inhibitors given their prominent MYB regulatory circuits. In contrast, somatic Notch activation might render grade 3 tumors relatively less sensitive to bromodomain inhibition, as recently observed in T-ALL with activating *NOTCH1* mutations[33]. We therefore examined the *in vivo* efficacy of BET inhibitors[34] in ACC primagrafts. To this end, we engrafted nude mice with 4 different ACCs, two grade 2 and two grade 3 tumors. We confirmed that both grade 3 primagrafts harbor genetic events leading to Notch activation (Supplementary Table 5), and stain strongly positive for ICN1 and the proliferation marker Ki-67 (Fig. 4a). Randomized groups of 5 mice each were treated with vehicle or the BET bromodomain inhibitor JQ1, and tumor growth was measured over time (Fig. 5a). BET inhibition significantly slowed tumor growth in the grade 2 primagrafts (Fig. 5b). We also detected a modest decrease in *MYB* and MYB target gene expression (Fig. 5c). In contrast, the grade 3 tumors did not respond to BET inhibition, potentially reflecting a relatively stronger dependency on Notch signaling. Of note, we recently showed that Notch-mutant ACCs are sensitive to Notch inhibitors[27]. Our results

suggest that BET inhibitors may be sufficient to disrupt core MYB circuitry in low grade ACC, but are ineffective against high grade tumors, which may instead be sensitive to Notch inhibitors.

Discussion

Adenoid cystic carcinoma is an incurable disease with slow but chronic tumor progression that is refractory to conventional chemotherapy or radiation. We have shown that most cases of ACC harbor translocations that juxtapose a super-enhancer to the *MYB* locus. A convergence of genetic, epigenetic and therapeutic data indicate that these rearrangements establish a positive feedback loop in which MYB protein binds the translocated enhancers, which in turn physically interact with the *MYB* promoter and drive its expression. Thus, although MYB is known to autoregulate itself in wildtype cells[35,36], enhancer hijacking events perturb this physiologic control in ACC, yielding a high degree of over-expression.

MYB coordinates with distinct regulatory programs in the alternate cell lineages in the cribriform grade 2 tumors, cooperating with a TP63 program in myoepithelial cells or a Notch program in luminal epithelial cells. In grade 3 tumors, however, additional genomic events frequently lead to constitutive Notch activation, and tip the balance towards the luminal epithelial fate, and a ‘solid’ histology. Grade 2 tumors appear dependent on bromodomain proteins to maintain MYB driven enhancer programs, as indicated by their sensitivity to the corresponding inhibitors. In contrast, grade 3 tumors with constitutive Notch activation are insensitive to bromodomain inhibitors, consistent with other Notch-driven tumors. In grade 2 tumors, IHC staining for MYB tends to be stronger in myoepithelial cells than in luminal cells, in line with previous reports[37,38], while grade 3 tumors exhibit diffuse MYB staining with variable intensity across tumors (Supplementary Fig. 9). Although these differences may in part reflect technical issues, they raise the possibility that lower MYB protein levels in grade 3 tumors influence tumor response to BET inhibitors. In conclusion, our study advances understanding of ACC biology, and underscores how interplay between genetic and epigenetic alterations can affect malignant transformation, disease progression, and therapeutic sensitivities.

Online Methods

Primary tumors

Primary adenoid cystic carcinomas were collected at MD Anderson Cancer Center, University of Virgina, and Massachusetts General Hospital with approval by the respective Institutional Review Boards.

Primagraft experiments

To generate adenoid cystic carcinoma primagrafts, viable adenoid cystic carcinoma cells were injected into the flank of nude (Foxn1^{nu}) mice. Tumors that grew were passaged through at least three rounds of nude transplantation prior to *in vivo* drug testing use. Studies were performed under the auspices of protocols approved by the University of Virginia IACUC[12].

For *in vivo* drug testing, 10^6 viable adenoid cystic carcinoma cells were injected into the flank of nude mice. Once tumor was visible, the mice were randomized to receive vehicle or JQ1 (50mg/kg daily) diluted in 10:90 DMSO:10%hydroxypropyl-beta-cyclodextrin orally until reaching minimal tumor volume of 1000 mm^3 (4 – 9 mice per group: X5M1 & X6 4 treated vs. 9 vehicle controls, X9 4 treated vs. 5 vehicle controls, X11 5 treated vs. 8 vehicle controls). Tumor growth was monitored and mice were weighed daily and sacrificed when moribund. In these experiments, no statistical methods were employed to determine the sample size, and no blinding of investigators was performed. All animal procedures used in this study were approved by the IACUC at START, Texas.

Cell lines

The HPV-transformed ACC cell line ACC112 was cultured in RPMI supplemented with 10% fetal bovine serum, Epidermal Growth Factor, Hydrocortisone and Insulin (all from R&D) as previously described [14]. Jurkat cells were obtained from ATCC and Oci-Ly3 cells from the Broad-Novartis Cancer Cell Line Encyclopedia. Both cell lines were cultured in RPMI with 10% fetal bovine serum and propagated at a density of 1 – 2 million cells per mL.

Calling *MYB* translocations

MYB translocations were called from paired-end whole genome sequencing data using the following datasets. Data of 12 primary tumors were obtained from the European Genome-phenome Archive, study EGAS00001000030. Out of the 12 tumors, 5 tumors were not considered for analysis due to low coverage or unreliable paired-end alignment. Data of 5 additional tumors were recently published and included in the analysis[7]. We performed 100bp paired end whole genome sequencing for 6 additional patient derived primagrafts with Illumina HiSeq. *MYB* translocation in the ACC primagrafts X5M1 and X11 were detected by paired end sequencing of H3K27ac ChIP-Seq and input control. All fastq files were aligned to the reference genome (hg19) using BWA ALN. Reads from primgrafts that align to the mouse genome (mm10) with maximal editing distance of 3bp (based on BWA alignment) were filtered out. Rearrangements were called with dRanger and BreakPointer[39,40]. Due to the lack of matching normal controls, we could not use the default germline filtering. Instead we have filtered against a panel of 100 non-matched normals, defining the rearrangement score as $10*q*t/\max(n,1)$, where q is the quality (as defined by dRanger), t the number of supporting read pairs in the tumor, and n the average number of supporting reads in the normals. Only rearrangement with score >= 5 were kept. Known germline variants from the DGV database[41] were filtered out. Intra-chromosomal rearrangements that span less than 1Mb were filtered out, as they were suspected to be germline. Rearrangements from ChIP-seq paired end data were called as previously described[42]. All *MYB* translocations were manually reviewed in IGV[43]. Only *MYB* and *NFIB* were found to have recurrent rearrangements in more than two primagrafts (even when considering all rearrangements with score >= 3). *CDH18, EYS* and *TAF13* were rearranged in two primagrafts, but not in the other 12 primary tumors. All new data has been deposited at the European Genome-phenome Archive (EGA), which is hosted by the EBI, under accession number EGAS00001001457.

Chromatin immunoprecipitation

We performed chromatin immunoprecipitation (ChIP) in primary tumors and primagrafts as described with the following modifications[44]. Frozen tissue was chopped up using a scalpel before fixation and then further dissociated after fixation by shearing with an 18G needle. Chromatin from formaldehyde-fixed cells (1–5 × 10^6 cells per histone mark, 10^7 cells for *MYB* binding) was fragmented to a size range of 200–700 bases with a Branson 250 Sonifier. Solubilized chromatin was immunoprecipitated with antibody against H3K4me3 (2.5 μl; Millipore, 07-473CA), H3K27ac (2.5 μl; Abcam, ab4729), MYB (10 μl; Bethyl, A304-136A) and TP63 (5 μl; ActiveMotif, #39739). Each of these antibodies was validated by protein blot or dot blot as described[45]. Antibody-chromatin complexes were pulled down with protein G magnetic beads (Dynabead, 10003D), washed and then eluted. After cross-link reversal and proteinase K treatment, immunoprecipitated DNA was treated with RNase and purified with Agencourt AMPure XP (Beckman Coulter A63880). Libraries were prepared according to Illumina's instructions. ChIP DNA and input controls were sequenced with the Illumina HiSeq 2500 or the NextSeq 500 instrument. Reads were aligned to the reference genome (hg19) using BWA[46]. Reads mapping to more than two genomic loci were ignored. Reads aligned to the same position and strand were only counted once. All data were deposited at the European Genome-phenome Archive (EGA), which is hosted by the EBI, under accession number EGAS00001001457.

Statistical analysis

Data for bone marrow derived mesenchymal stem cells and gastric and fetal leg muscle tissues are publicly available through the Roadmap Program (GSM1112792, GSM1013128, GSM1058767); HMEC, PANC1 and MCF7 cell line data were downloaded from ENCODE (GSM733660, GSM818826, GSM945854); data for MGG28 and Ewing sarcoma were recently published[47,48]; MOLT3 data were taken from[19].

Peaks and motifs were called using HOMER[49]. H3K27ac peaks were centered on nucleosome free regions, set to be 400bp with a minimal distance of 600bp, and required to be 4 fold more than matching input. MYB peaks were called with default parameters. To call putative super-enhancers, BRD4 or H3K27ac peaks up to 12.5kb apart were stitched together, and enhancers with a slope greater than 1 were considered super enhancers, as described in reference[15]. H3K27ac heat maps were calculated after merging all H3K27ac peaks across samples. Signal was normalized by total signal per sample. Only peaks with normalized signal > 10 fpm in at least one sample were considered. Inter-sample correlations were calculated by Spearman's rho. Motifs were called with HOMER in a 300bp region around the peak center. To identify top H3K27ac motifs, known motifs were sorted based on median p-value across all samples. To identify differential motifs between grades, we merged H3K27ac of all grade 2 and all grade 3 primagrafts, and then defined peaks with more than 4 fold higher signal, averaging across 2kb regions in one over the other set.

High confidence MYB peaks were called by merging peaks from 3 grade 2 primagrafts, summing MYB signal over each peak in each sample, normalizing each sample by the average signal of that sample, and selecting peaks where the average signal over all samples

was at least 0.75. To determine which genes are expressed we used published microarray data[12], averaging over the 3 samples (log_2 space). Any gene with an average expression level greater than 5 was considered to be expressed. Peaks were assigned to genes using GREAT[50], limited to 100kb maximal distance. We calculated GOBP[51], MSigDB[52] and REACTOME[53] annotation enrichment of all MYB bound and expressed genes versus all expressed genes using Fisher exact test (FDR < 1%). To identify MYB driven transcriptional regulators we focused on targets annotated as "positive regulation of transcription, DNA-templated" by GOBP (GO:0045893) that were found to be significantly enriched ($p<3.8 x10^{-7}$) in the analysis above. We then ranked all those genes by total normalized MYB signal on all MYB peaks assigned to the respective gene. Normal salivary gland RNA-seq data were obtained from the human protein atlas (HPA)[20]. Genes were divided into "not detected", "low" or "high", based on HPA definitions, where "high" includes both "medium" and "high" genes of HPA definitions. Annotation enrichment of expressed MYB targets in a given set was compared to all genes in that set that are expressed in ACC. To test expression of MYB targets and non-MYB targets we compared the average expression of the expressed MYB targets in ACC as described above to the average expression of other expressed ($log_2 \geq 5$) genes. To control for MYB independent expression differences between those genes we compared the expression of the same sets of genes in normal salivary gland. To compare MYB binding profiles to previously published promoters bound by MYB in MCF7 cells[17], we compared it to the subset of our high confidence MYB peaks above at most 2kb from TSS. To compare these MYB binding profiles to previously published MYB profiles for mouse myeloid progenitors[18], we compared bound genes in mouse (as listed there in Supplementary Tables 5 and 6) to homologous human genes (by NCBI's HomoloGene), with assigned high confidence MYB peak in ACC. To estimate BRD4 overlap with MYB peaks, we called MYB and BRD4 signal on all MYB peaks detected in ACCX5M1 and ACCX9, and counted peaks with normalized binding > 30 fpm. To estimate TP63 overlap with MYB peaks we called MYB and TP63 signal on all TP63 peaks detected in ACCX5M1 and count peaks with normalized binding > 30 fpm.

To quantify MYB signal over enhancers per target gene, MYB peaks more than 2kb away from the TSS were assigned to genes using GREAT, limiting maximal distance to 1Mb to allow for fair comparison of the wide range of translocated NFIB enhancers. We then compared the total MYB signal over the translocated enhancers to the total signal over all enhancers of any MYB target.

Significance of 3C analysis was called based on 95% confidence interval not intersecting zero interaction. Significance of JQ1 treatment in primagraft experiments was called by one-tailed student's t-test at the last time point for which tumor measurements were obtained. Significance of qPCR after JQ1 treatment was called by one-tailed student's t-test between JQ1 treated and vehicle.

Quantitative RT-PCR analyses

Frozen tumor tissue was mechanically homogenized and total RNA was extracted with Trizol (Life Technologies) followed by the RNeasy Mini Kit (Qiagen) with on-the-column DNase treatment. Total RNA was reverse transcribed into cDNA using the SuperScript III

First-Strand Synthesis system for RT-PCR. qPCR was performed with FastStart Universal SYBR Green Master (Roche) on an ABI 7500 (primer sequences are listed in Supplementary Table 6). Gene expression was measured by determining the $\log_2(C_t)$ value of the desired transcript compared to *GAPDH* transcript. A one-tailed p-value < 0.05 was considered statistically significant.

Genomic breakpoint PCR analyses

For validation of genomic rearrangements, genomic DNA was extracted from ACC primagrafts using the QiaAmp DNA mini kit (Qiagen). PCR reactions were performed with 2 min extension times to allow for adequate amplification of longer fragments. PCR products were visualized on a 1.5% agarose gel. MYB rearrangements, and representative highest confidence and lowest confidence rearrangements were selected for validation (See Supplementary Table 1). Rearrangements in 4 primagrafts were validated. The primer sequences are listed in Supplementary Table 6.

Reporter assays

Five translocated enhancer sequences and five controls with scrambled MYB consensus motifs (replacing CNGTT with GTAAG, see Supplementary Table 6) were synthesized and cloned into the pGL 4.23 [luc2/minP] vector (Promega) by BlueHeron. Enhancer activity was measured in 6 replicates as relative luminescence of the pGL 4.23 [luc2/minP] vector compared to the pGL 4.73 [hRluc/SV40] with Dual-Glo Luciferase (Promega) after a 36 hour co-nucleofection into Jurkat cells following the manufacturer's instructions (Amaxa cell line nucleofactor kit V from Lonza).

Chromosome Conformation Capture

Chromosome Conformation Capture was performed as described[54]. In brief, frozen tumor tissue was chopped up using a scalpel before fixation and then further dissociated after fixation by shearing with an 18G needle. Cross-linked chromatin was then digested with 500U of HindIII (Roche) overnight at 37°C followed by ligation. 3C products were phenol/chloroform extracted, ethanol-precipitated, and dissolved in Tris/EDTA buffer. Each PCR was performed under the following conditions: 95°C for 10 minutes; 65 cycles at 95°C for 15 seconds; 60°C for 1 minute; 72°C for 1 minute; and a final extension at 72°C for 10 minutes. PCR products were analyzed by agarose gel electrophoresis. Primer and TaqMan probe sequences are listed in Supplementary Table 6. Any undetected qPCR call, or Ct>50 were considered as Ct=50. 95% confidence intervals were used to call statistical significance.

Immunohistochemistry

Formalin fixed paraffin embedded sections were cut at 4 microns and place on Superfrost plus glass slides, which were were baked for 60 minutes at 60° C. Staining was conducted on a Leica Bond III automated immunohistochemical staining work station. To stain for MYB, antigen retrieval was performed using Bond Epitope Retrieval 1 solution for 30 minutes. Staining was carried out by incubation with a MYB-specific rabbit monoclonal primary antibody (EP769Y, Abcam, ab45150) at 1:400 for 30 minutes at room temperature,

followed by incubation with a rabbit-specific secondary antibody linked to horseradish peroxidase (Bond Polymer Refine Detection kit). Staining was developed by incubation with diaminobenzamidine (Leica Detection Kit), and slides were then dehydrated and coverslipped. Dual staining for activated NOTCH1 (ICN1) and p63 was carried out by first performing antigen retrieval using Bond Epitope Retrieval 2 solution for 40 minutes. Slides were then incubated with ICN1 antibody (D3B8, Cell Signaling Technologies, #4147) at 1:100 for 60 minutes at room temperature, followed by incubation with a rabbit-specific secondary antibody linked to horseradish peroxidase (Bond Polymer Refine Detection kit). ICN1 staining was then developed by incubation with diaminobenzamidine (Leica Detection Kit). Slides were then incubated in a second primary antibody, a murine monoclonal antibody specific for p63 (4A4, Biocare, CM163A) at 1:250 for 30 minutes. The second antibody was detected using the murine specific Bond Polymer Refine Red Detection kit, which detects staining using Fast Red, part of the detection kit. Slides were then dehydrated and coverslipped. Dual staining for ICN1 and KIT was performed as above, using a rabbit monoclonal antibody specific for ICN1 (D3B8, Cell Signaling Technologies, #4147) at 1:100 for 60 minutes at room temperature, and a second primary antibody, a murine monoclonal antibody specific for KIT (Dako, A4502), at 1:250 for 30 minutes.

To generate spectral libraries, single-stained tissue sections were imaged using the Mantra multispectral imaging platform (PerkinElmer, Hopkinton, MA). The spectrally resolved, individual profiles between 420–720 nm of 3,3′-diaminobenzidine (DAB; ICN1), fast red (KIT or p63), and the haematoxylin counterstain were used to deconvolute staining patterns in triple-stained tissue sections. Three representative areas of each stained tissue section were imaged at 20x magnification and deconvoluted using the Inform 2.1 software package (PerkinElmer). Each image was manually divided into tumor and stromal tissue, and individual tumor cells were segmented using Inform 2.1 algorithms that score positive staining of nuclei and cell membranes for each color.

Supplementary Material

Refer to Web version on PubMed Central for supplementary material.

Acknowledgments

We thank M. Rivera, N. Riggi, S. Puram, P. van Galen, J. Lohr and J. Kaufman for helpful discussions and critical comments on the manuscript; J. Voisine, R. Isenhart, R. Issner, H. Whitton, A. Spooner, M. Uziel, C. Epstein, N. Shoresh, and the Broad Genome Sequencing Platform for technical assistance; T. Chan and V. Makarov for help with WGS data access; and The Salivary Gland Tumor Biorepository for providing the primary tumors (NIDCR Award Reference Number HHSN268200900039C 04). This work was supported by the Adenoid Cystic Carcinoma Research Foundation (B.E.B; B.K.), the Temares Family Foundation, and the Howard Hughes Medical Institute. B.E.B. is an American Cancer Society Research Professor.

References

1. Ohno H, et al. Molecular analysis of a chromosomal translocation, t(9;14)(p13;q32), in a diffuse large-cell lymphoma cell line expressing the Ki-1 antigen. Proc Natl Acad Sci U S A. 1990; 87:628–32. [PubMed: 2153959]
2. Rabbitts TH. Chromosomal translocations in human cancer. Nature. 1994; 372:143–9. [PubMed: 7969446]

3. Groschel S, et al. A single oncogenic enhancer rearrangement causes concomitant EVI1 and GATA2 deregulation in leukemia. Cell. 2014; 157:369–81. [PubMed: 24703711]
4. Northcott PA, et al. Enhancer hijacking activates GFI1 family oncogenes in medulloblastoma. Nature. 2014; 511:428–34. [PubMed: 25043047]
5. Tomlins SA, et al. Recurrent fusion of TMPRSS2 and ETS transcription factor genes in prostate cancer. Science. 2005; 310:644–8. [PubMed: 16254181]
6. Adelstein DJ, Koyfman SA, El-Naggar AK, Hanna EY. Biology and management of salivary gland cancers. Semin Radiat Oncol. 2012; 22:245–53. [PubMed: 22687949]
7. Ho AS, et al. The mutational landscape of adenoid cystic carcinoma. Nat Genet. 2013; 45:791–8. [PubMed: 23685749]
8. Ramsay RG, Gonda TJ. MYB function in normal and cancer cells. Nat Rev Cancer. 2008; 8:523–34. [PubMed: 18574464]
9. Persson M, et al. Recurrent fusion of MYB and NFIB transcription factor genes in carcinomas of the breast and head and neck. Proc Natl Acad Sci U S A. 2009; 106:18740–4. [PubMed: 19841262]
10. Mitani Y, et al. Comprehensive analysis of the MYB-NFIB gene fusion in salivary adenoid cystic carcinoma: Incidence, variability, and clinicopathologic significance. Clin Cancer Res. 2010; 16:4722–31. [PubMed: 20702610]
11. Stephens PJ, et al. Whole exome sequencing of adenoid cystic carcinoma. J Clin Invest. 2013; 123:2965–8. [PubMed: 23778141]
12. Moskaluk CA, et al. Development and characterization of xenograft model systems for adenoid cystic carcinoma. Lab Invest. 2011; 91:1480–90. [PubMed: 21709671]
13. Rivera CM, Ren B. Mapping human epigenomes. Cell. 2013; 155:39–55. [PubMed: 24074860]
14. Queimado L, et al. In vitro transformation of cell lines from human salivary gland tumors. Int J Cancer. 1999; 81:793–8. [PubMed: 10328235]
15. Whyte WA, et al. Master transcription factors and mediator establish super-enhancers at key cell identity genes. Cell. 2013; 153:307–19. [PubMed: 23582322]
16. Loven J, et al. Selective inhibition of tumor oncogenes by disruption of super-enhancers. Cell. 2013; 153:320–34. [PubMed: 23582323]
17. Quintana AM, Liu F, O'Rourke JP, Ness SA. Identification and regulation of c-Myb target genes in MCF-7 cells. BMC Cancer. 2011; 11:30. [PubMed: 21261996]
18. Zhao L, et al. Integrated genome-wide chromatin occupancy and expression analyses identify key myeloid pro-differentiation transcription factors repressed by Myb. Nucleic Acids Res. 2011; 39:4664–79. [PubMed: 21317192]
19. Mansour MR, et al. Oncogene regulation. An oncogenic super-enhancer formed through somatic mutation of a noncoding intergenic element. Science. 2014; 346:1373–7. [PubMed: 25394790]
20. Uhlen M, et al. Proteomics. Tissue-based map of the human proteome. Science. 2015; 347:1260419. [PubMed: 25613900]
21. Bell D, Bell A, Roberts D, Weber RS, El-Naggar AK. Developmental transcription factor EN1--a novel biomarker in human salivary gland adenoid cystic carcinoma. Cancer. 2012; 118:1288–92. [PubMed: 21800291]
22. Yamamoto Y, Saka T, Makimoto K, Takahashi H. Histological changes during progression of adenoid cystic carcinoma. J Laryngol Otol. 1992; 106:1016–20. [PubMed: 1336026]
23. Sato K, et al. Adenoid cystic carcinoma of the maxillary sinus with gradual histologic transformation to high-grade adenocarcinoma: a comparative report with dedifferentiated carcinoma. Virchows Arch. 2006; 448:204–8. [PubMed: 16133359]
24. Barbareschi M, et al. p63, a p53 homologue, is a selective nuclear marker of myoepithelial cells of the human breast. Am J Surg Pathol. 2001; 25:1054–60. [PubMed: 11474290]
25. Nguyen BC, et al. Cross-regulation between Notch and p63 in keratinocyte commitment to differentiation. Genes Dev. 2006; 20:1028–42. [PubMed: 16618808]
26. Yalcin-Ozuysal O, et al. Antagonistic roles of Notch and p63 in controlling mammary epithelial cell fates. Cell Death Differ. 2010; 17:1600–12. [PubMed: 20379195]
27. Stoeck A, et al. Discovery of Biomarkers Predictive of GSI Response in Triple-Negative Breast Cancer and Adenoid Cystic Carcinoma. Cancer Discov. 2014; 4:1154–67. [PubMed: 25104330]

28. Robinson DR, et al. Functionally recurrent rearrangements of the MAST kinase and Notch gene families in breast cancer. Nat Med. 2011; 17:1646–51. [PubMed: 22101766]
29. Haydu JE, et al. An activating intragenic deletion in NOTCH1 in human T-ALL. Blood. 2012; 119:5211–4. [PubMed: 22510873]
30. Moll UM, Slade N. p63 and p73: roles in development and tumor formation. Mol Cancer Res. 2004; 2:371–86. [PubMed: 15280445]
31. Mitani Y, et al. Expression and regulation of the DeltaN and TAp63 isoforms in salivary gland tumorigenesis clinical and experimental findings. Am J Pathol. 2011; 179:391–9. [PubMed: 21703418]
32. Roe JS, Mercan F, Rivera K, Pappin DJ, Vakoc CR. BET Bromodomain Inhibition Suppresses the Function of Hematopoietic Transcription Factors in Acute Myeloid Leukemia. Mol Cell. 2015; 58:1028–39. [PubMed: 25982114]
33. Knoechel B, et al. An epigenetic mechanism of resistance to targeted therapy in T cell acute lymphoblastic leukemia. Nat Genet. 2014; 46:364–70. [PubMed: 24584072]
34. Filippakopoulos P, et al. Selective inhibition of BET bromodomains. Nature. 2010; 468:1067–73. [PubMed: 20871596]
35. Nicolaides NC, Gualdi R, Casadevall C, Manzella L, Calabretta B. Positive autoregulation of c-myb expression via Myb binding sites in the 5′ flanking region of the human c-myb gene. Mol Cell Biol. 1991; 11:6166–76. [PubMed: 1944282]
36. Nomura T, et al. Negative autoregulation of c-Myb activity by homodimer formation through the leucine zipper. J Biol Chem. 1993; 268:21914–23. [PubMed: 8408047]
37. Brill LB 2nd, et al. Analysis of MYB expression and MYB-NFIB gene fusions in adenoid cystic carcinoma and other salivary neoplasms. Mod Pathol. 2011; 24:1169–76. [PubMed: 21572406]
38. Bell D, et al. Clinical significance of Myb protein and downstream target genes in salivary adenoid cystic carcinoma. Cancer Biol Ther. 2011; 12:569–73. [PubMed: 21785271]
39. Berger MF, et al. The genomic complexity of primary human prostate cancer. Nature. 2011; 470:214–20. [PubMed: 21307934]
40. Drier Y, et al. Somatic rearrangements across cancer reveal classes of samples with distinct patterns of DNA breakage and rearrangement-induced hypermutability. Genome Res. 2013; 23:228–35. [PubMed: 23124520]
41. MacDonald JR, Ziman R, Yuen RK, Feuk L, Scherer SW. The Database of Genomic Variants: a curated collection of structural variation in the human genome. Nucleic Acids Res. 2014; 42:D986–92. [PubMed: 24174537]
42. Ryan RJ, et al. Detection of Enhancer-Associated Rearrangements Reveals Mechanisms of Oncogene Dysregulation in B-cell Lymphoma. Cancer Discov. 2015; 5:1058–71. [PubMed: 26229090]
43. Thorvaldsdottir H, Robinson JT, Mesirov JP. Integrative Genomics Viewer (IGV): high-performance genomics data visualization and exploration. Brief Bioinform. 2013; 14:178–92. [PubMed: 22517427]
44. Ku M, et al. Genomewide analysis of PRC1 and PRC2 occupancy identifies two classes of bivalent domains. PLoS Genet. 2008; 4:e1000242. [PubMed: 18974828]
45. Ernst J, et al. Mapping and analysis of chromatin state dynamics in nine human cell types. Nature. 2011; 473:43–9. [PubMed: 21441907]
46. Li H, Durbin R. Fast and accurate short read alignment with Burrows-Wheeler transform. Bioinformatics. 2009; 25:1754–60. [PubMed: 19451168]
47. Suva ML, et al. Reconstructing and reprogramming the tumor-propagating potential of glioblastoma stem-like cells. Cell. 2014; 157:580–94. [PubMed: 24726434]
48. Riggi N, et al. EWS-FLI1 utilizes divergent chromatin remodeling mechanisms to directly activate or repress enhancer elements in Ewing sarcoma. Cancer Cell. 2014; 26:668–81. [PubMed: 25453903]
49. Heinz S, et al. Simple combinations of lineage-determining transcription factors prime cis-regulatory elements required for macrophage and B cell identities. Mol Cell. 2010; 38:576–89. [PubMed: 20513432]

50. McLean CY, et al. GREAT improves functional interpretation of cis-regulatory regions. Nat Biotechnol. 2010; 28:495–501. [PubMed: 20436461]

51. Ashburner M, et al. Gene ontology: tool for the unification of biology. The Gene Ontology Consortium. Nat Genet. 2000; 25:25–9. [PubMed: 10802651]

52. Subramanian A, et al. Gene set enrichment analysis: a knowledge-based approach for interpreting genome-wide expression profiles. Proc Natl Acad Sci U S A. 2005; 102:15545–50. [PubMed: 16199517]

53. Milacic M, et al. Annotating cancer variants and anti-cancer therapeutics in reactome. Cancers (Basel). 2012; 4:1180–211. [PubMed: 24213504]

54. Deng W, et al. Controlling long-range genomic interactions at a native locus by targeted tethering of a looping factor. Cell. 2012; 149:1233–44. [PubMed: 22682246]

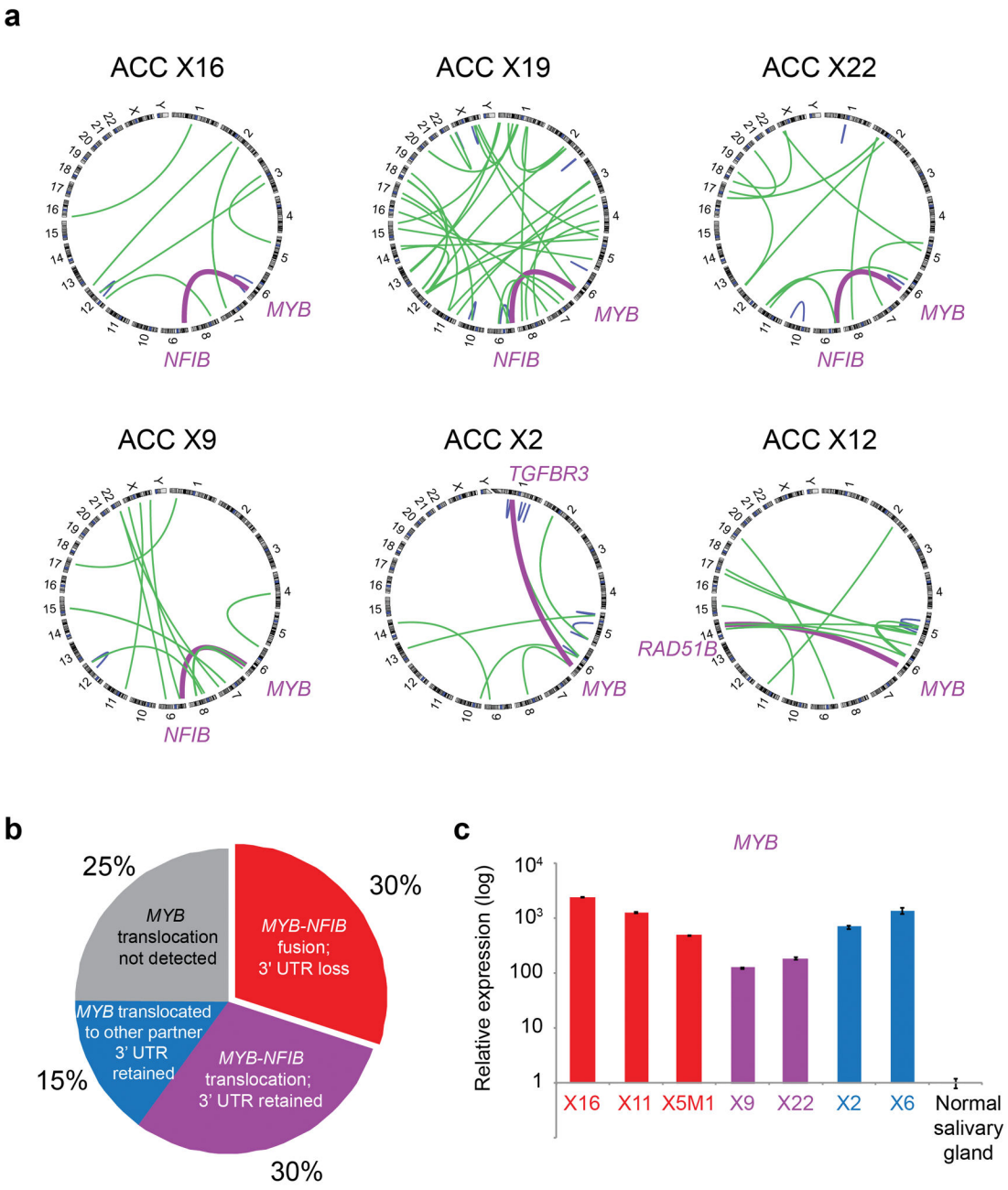

Figure 1. MYB translocations involve alternate partners and frequently retain the 3′ UTR

a. Circos plots of inter-chromosomal translocations in 6 ACC primagrafts. Only *MYB* translocations (marked in purple) occur in more than 2 tumors. **b.** For a cohort of 20 tumors, pie chart depicts fraction of *MYB* translocations that involve the *NFIB* locus, with or without loss of the *MYB* 3′UTR, or that rearrange to other loci (*TGFBR3* or *RAD51B*). These rearrangements to alternative partners retain the *MYB* 3′UTR. **c.** Log plot shows *MYB* mRNA expression in ACC primagrafts, relative to normal salivary gland. Error bars reflect standard error of means (SEM, n=3 experiments per sample); $p < 10^{-5}$ compared to

normal in all cases. These data suggest that neither UTR loss nor NFIB fusion is sufficient to explain robust *MYB* overexpression in ACC.

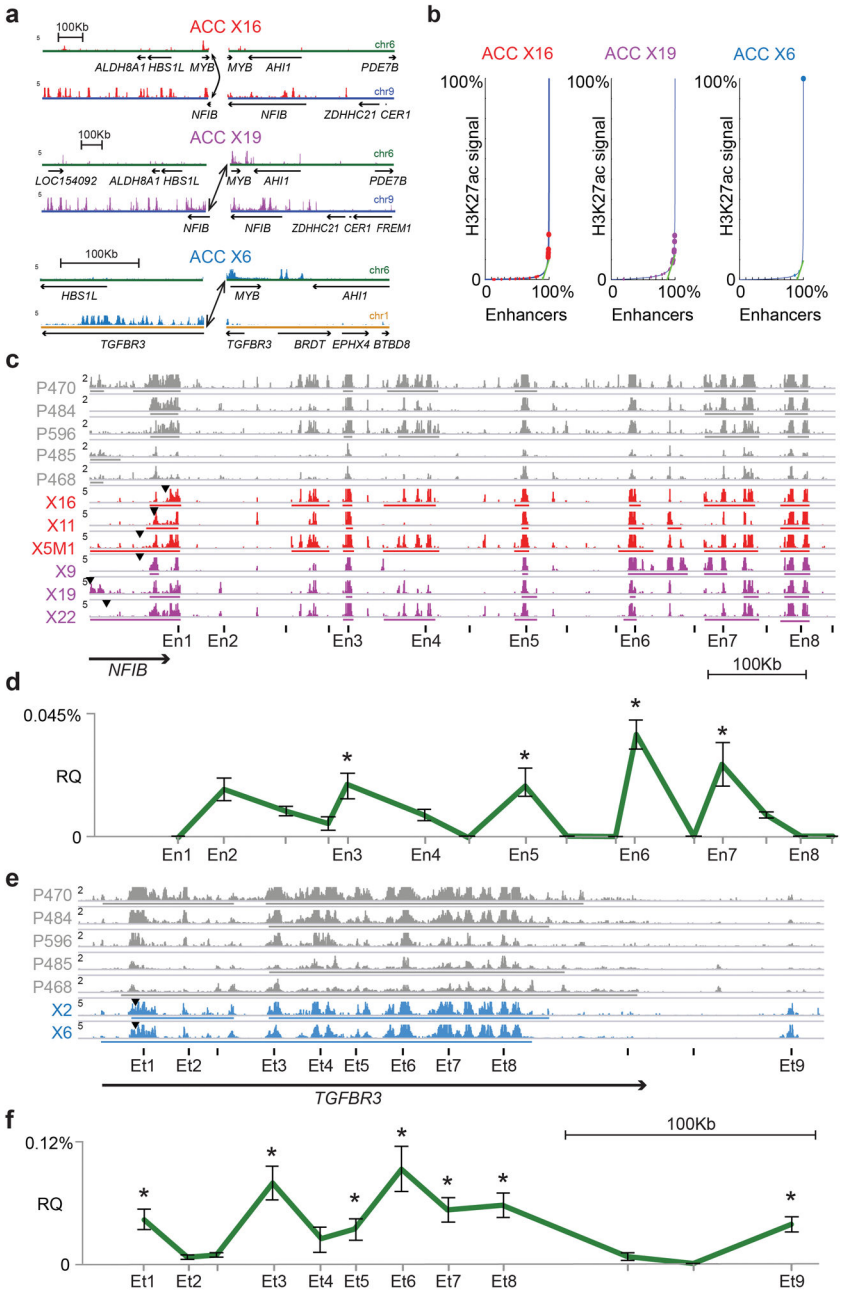

Figure 2. Translocation partners contain super-enhancers that loop to the MYB promoter

a. H3K27ac (enhancer) profiles are shown for alternate ACC rearrangements: *MYB-NFIB* translocation with loss of *MYB* 3′UTR (X16); *MYB-NFIB* translocation with retained 3′UTR (X19); and *MYB-TGFBR3* translocation with retained *MYB* 3′UTR (X6). Arrows indicate the rearrangements. H3K27ac signal is scaled in fragments per million. **b.** Candidate enhancers ranked by H3K27ac signal in ACC primagrafts diagramed in Panel a. Expansive enhancers in the *NFIB* (red and purple) and *TGFBR3* (blue) loci satisfy super-enhancer criteria. These enhancers score similarly in other tumors (Supplementary Fig. 3). **c.** H3K27ac (enhancer) profiles for the *NFIB* locus (negative strand shown) in 5ACCs and 6

MYB-NFIB positive primagrafts. Enhancers are numbered as indicated (En1–En8). Translocations occur close to the 5′UTR of *NFIB* near the En1 enhancer (black triangles). Bars below peaks mark super-enhancers. **d**. Chromosome Conformation Capture (3C) demonstrates looping of translocated enhancers to *MYB* promoter in X19. The plot depicts, for each enhancer (En1–En8) or control site, its normalized interaction frequency with the *MYB* promoter. Significant interactions ($p<0.05$) are marked by '*', and error bars show SEM (n=5). **e.** H3K27ac profiles for the *TGFBR3* locus (negative strand) in 5 ACCs and 2 *MYB-TGFBR3* positive primagrafts. Translocations occur within *TGFBR3*, near the Et1 enhancer (black triangles). **f.** 3C demonstrates looping of translocated enhancers to *MYB* promoter in X6 (*MYB-TGFBR3* rearrangement), as in Panel d. Error bars show SEM (n=5). These data suggest that alternate ACC rearrangements juxtapose super-enhancers to the *MYB* locus that physically interact with the *MYB* promoter, and activate its expression.

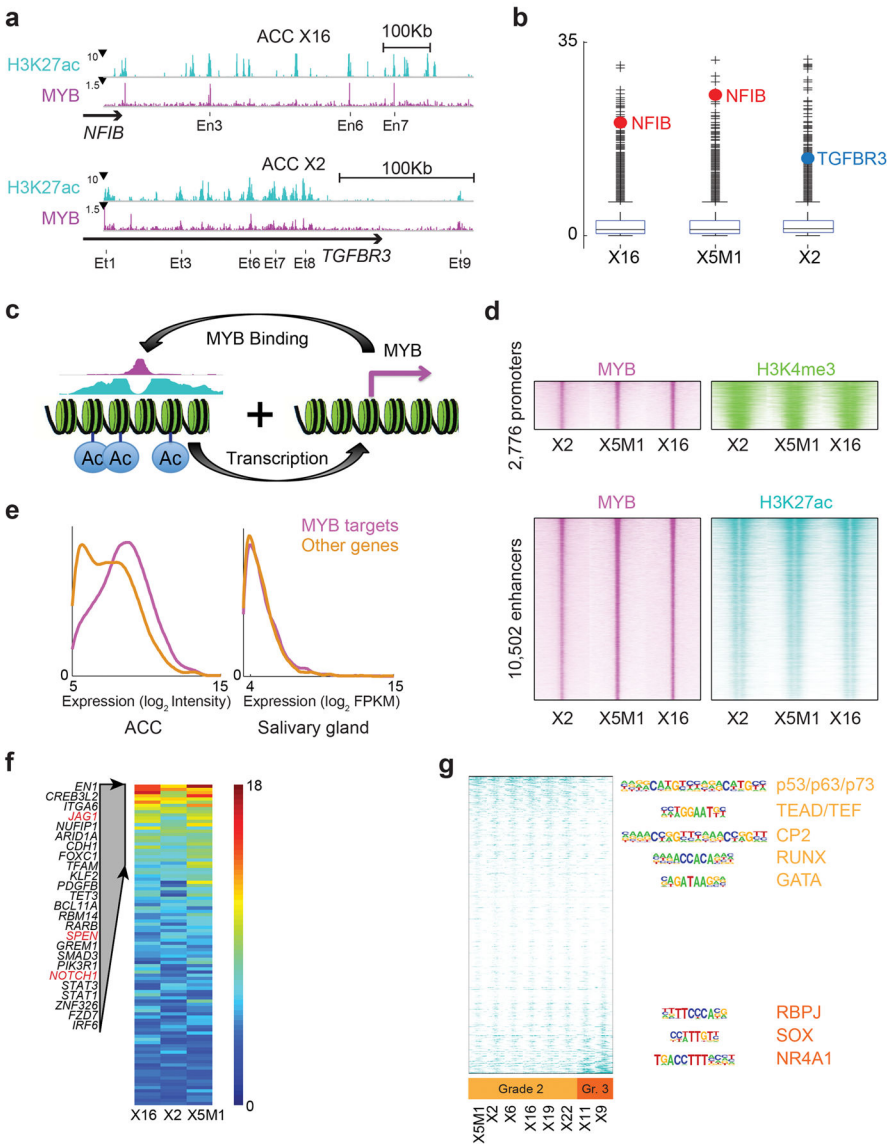

Figure 3. MYB protein binds translocated super-enhancers and other active enhancers

a. MYB binding and H3K27ac profiles are shown for the *NFIB* locus in X16 or the *TGFBR3* locus in X2 (negative strand shown). MYB-bound enhancers looping to MYB promoter are labeled as in Figure 2c–f. **b**. Box plot depicts distribution of MYB signal over enhancers in ACCs. Box shows quartiles (*q*1, *q*2, *q*3), whiskers extending to *q*3+*1.5**(*q*3 *q*1). Super-enhancers in the *NFIB* locus are top-ranked MYB targets in tumors with *MYB-NFIB* translocation (red points; #5 in X5M1, #17 in X16). Super-enhancers in the *TGFBR3* locus are top-ranked MYB targets in tumors with *MYB-TGFBR3* (#77 in X2). **c.** Schematic depicts positive feedback loop, engaged by chromosomal rearrangements, that sustains *MYB* overexpression in ACC. **d.** High confidence *MYB* peaks in three grade 2 primagrafts (see methods) were annotated as ‘promoter’ (+/− 2kb from TSS; top) or ‘enhancer’ (bottom). Heat maps show MYB and H3K4me3 signals over 2776 promoters (rows; 5Kb regions centered on MYB peaks, ranked by MYB signal), or MYB and H3K27ac signals

over 10502 enhancers (rows; 5Kb regions centered on MYB peaks, ranked by MYB signal). **e**. Expression of MYB target genes, compared to control genes, in ACC primagrafts (left) and normal salivary gland (right). High expression of genes near MYB binding sites supports a role for MYB as a transcriptional activator in ACC. **f**. MYB target genes ranked by cumulative MYB signal over promoter and nearby enhancers (Notch pathway genes in red). **g.** Heat map shows enhancers with preferential H3K27 acetylation in grade 2 (top) or grade 3 (bottom) primagrafts. TF motifs enriched in the respective enhancer groups are indicated.

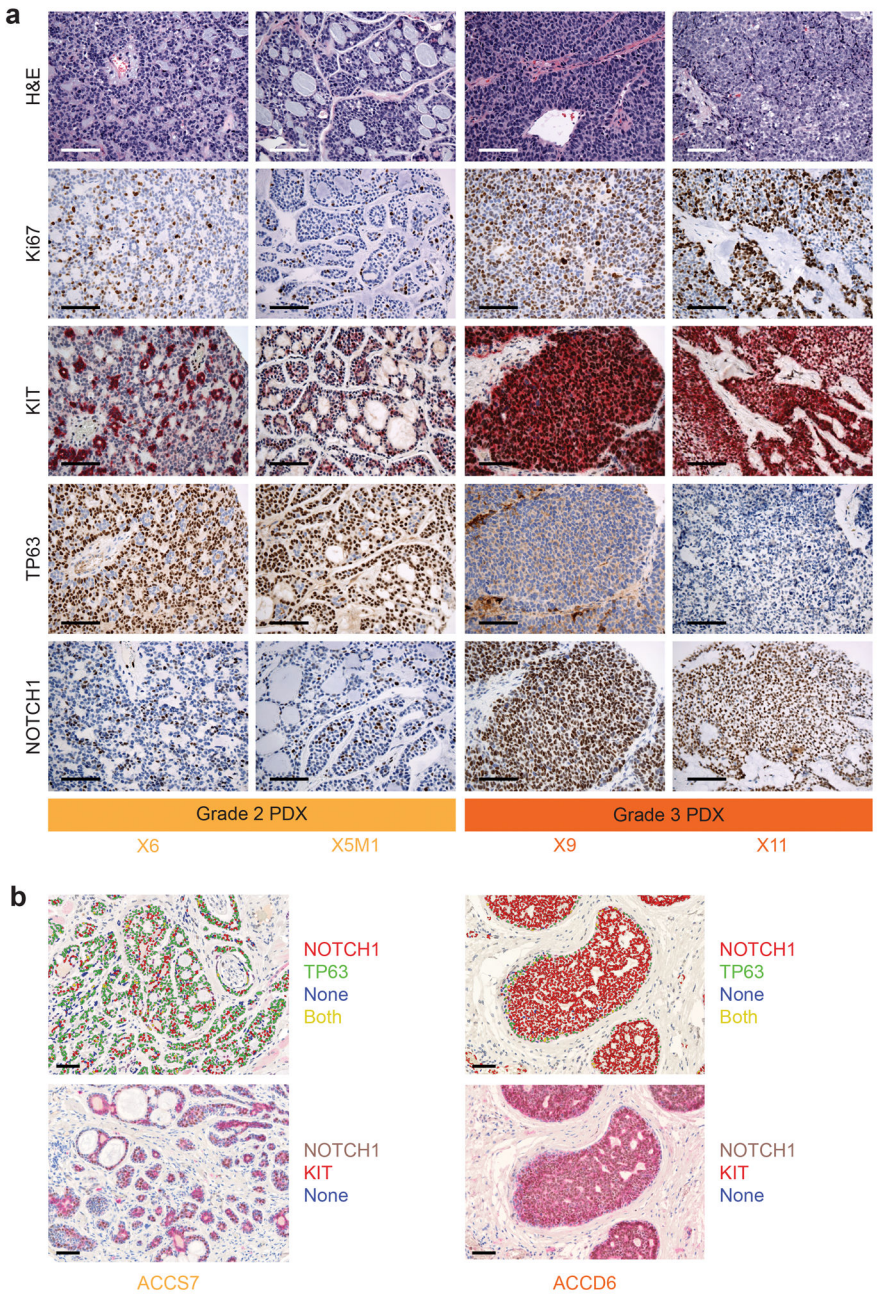

Figure 4. MYB drives alternate cell fates in ACC

a. Images show H&E stains and immunohistochemistry for Ki-67, KIT, TP63 and activated NOTCH1 (ICN1) in two grade 2 and two grade 3 primagrafts. Scale bar is 100μm. Grade 2 tumors have a cribriform histology with a mixture of myoepithelial (TP63) and luminal epithelial cells (KIT, ICN1). Grade 3 tumors show strong Notch activation with loss of myoepithelial cells (TP63). **b.** Co-staining of ICN1 and TP63 or ICN1 and KIT in a grade 2 ACC (top 2 panels) and grade 3 ACC (bottom 2 panels). Scale bar is 100μm. Expression of ICN1 and TP63 are almost always mutually exclusive.

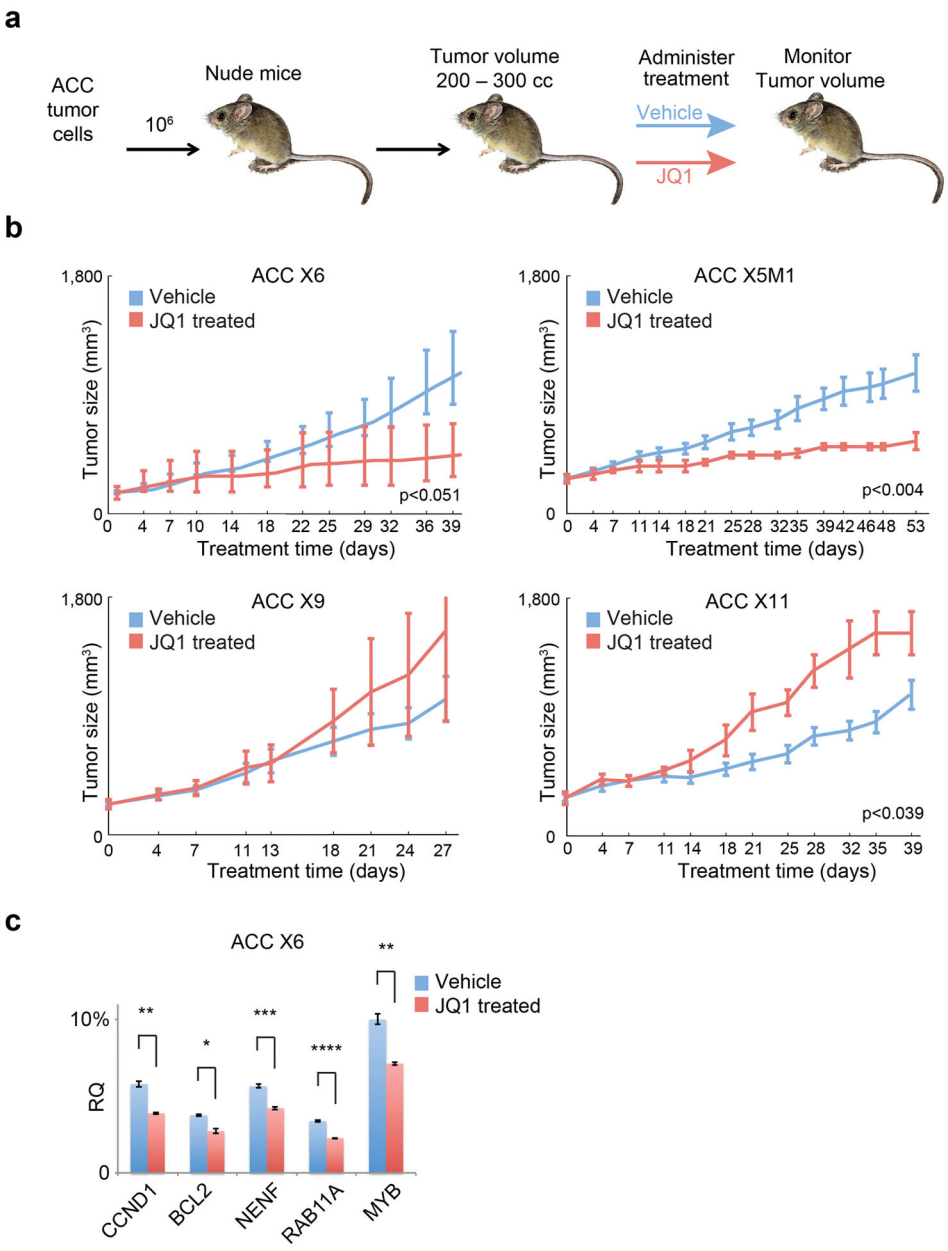

Figure 5. BET inhibition slows tumor growth in grade 2 ACC primagrafts

a. Experimental design for ACC xenotransplantation trials with the BET bromodomain inhibitor JQ1. ACC cells from four different human tumors were transplanted into the flanks of nude mice. Once tumor size reached 200 – 300 cc, mice were randomized into 2 treatment groups (vehicle or JQ1). Mice were treated daily, and were monitored for disease burden. The trial was stopped when mice became moribund. **b.** Average tumor size from 3–9 mice per group is depicted during the period of the xenotransplantation trial (Grade 2 tumors: X6, X5M1; grade 3 tumors: X9, X11). Error bars show standard error of means. **c.** Plot shows mRNA expression of *MYB* and selected MYB target genes after JQ1 treatment (normalized to GAPDH; * = $p<10^{-2}$, ** = $p<10^{-3}$, *** = $p<10^{-4}$, **** = $p<10^{-5}$; error bars

show standard error of means, n=3). BET inhibition slows growth and leads to downregulation of *MYB* and MYB target genes in grade 2 tumors.

Table 1

***MYB* translocations**

MYB translocations as detected in 12 primary ACCs and 8 primagrafts. The source of the samples is 1. WGS data from the European Genome-phenome Archive, dataset EGAD00001000062, 2. WGS data from Ho et al.[7], 3. WGS conducted in this study, 4. Paired-end ChIP-seq of H3K27ac and input control conducted in this study.

Sample	Origin	*MYB* translocation	*MYB* 3′UTR	Source	Remarks
PD3185	Primary	Not detected		1	
PD3186	Primary	Not detected		1	Low coverage
2012	Primary	Not detected		2	
2128	Primary	Not detected		2	
6536	Primary	Not detected		2	
PD3176a	Primary	*MYB-NFIB* fusion	Lost	1	Inversion
PD3208a	Primary	*MYB-NFIB* fusion	Lost	1	Inversion
505	Primary	*MYB-NFIB* fusion	Lost	2	Inversion
131169	Primary	To *NFIB* locus	Retained	2	
PD3226a	Primary	To *NFIB* locus	Retained	1	Complex
PD5912a	Primary	To *NFIB* locus	Retained	1	Complex
PD3177a	Primary	To *TGFBR3* locus	Retained	1	
ACCX5M1	Primagraft	*MYB-NFIB* fusion	Lost	4	Inversion
ACCX11	Primagraft	*MYB-NFIB* fusion	Lost	4	Inversion
ACCX16	Primagraft	*MYB-NFIB* fusion	Lost	3	Inversion
ACCX9	Primagraft	To *NFIB* locus	Retained	3	
ACCX19	Primagraft	To *NFIB* locus	Retained	3	
ACCX22	Primagraft	To *NFIB* locus	Retained	3	
ACCX2	Primagraft	To *TGFBR3* locus	Retained	3	
ACCX12	Primagraft	To *RAD51B* locus	Retained	3	

Table 2

MYB, Notch and TP63 immunohistochemistry

Tumors of all grades express MYB in all cells, while grade 3 have strong intercellular NOTCH1 (ICN1) stains but no TP63 expression, as opposed to grade 1 and 2 tumors, expressing TP63 in some cells and Notch in some (unk = unkown).

Tumor	MYB	ICN1	TP63	Grade	Tumor Site
ACCD1	Diffuse +	Diffuse +	Minor subset +, periphery (<5%)	3	Trachea
ACCD2	Diffuse +	Diffuse +	Minor subset +, periphery (<5%)	3	Parotid
ACCD3	Diffuse +	Diffuse +	Minor subset +, periphery (<5%)	3	Trachea
ACCD4	Diffuse +	Diffuse +	Negative	3	Maxillary Sinus
ACCD5	Diffuse +	Diffuse +	Negative	3	Trachea
ACCS1	70% +	60% +	40% +	2	Parotid
ACCS2	Staining failed	60% +	30%	2	Trachea
ACCS3	60% +	10% +	90% +	2	Parotid
ACCS4	70% +	30% +	70% +	2	Auditory Canal
ACCS5	90% +	50% +	20% +	2	Parotid
ACCS6	80% +	40% +	60% +	2	Parotid
ACCX2	N/A	20%	50%	2	Parotid
ACCX5M1	N/A	30%	80%	2	Metastatic tumor to lungs
ACCX6	N/A	30%	80%	2	Metastatic tumor to lungs
ACCX9	N/A	100%	0	3	Parotid
ACCX11	N/A	100%	0	3	Sinonasal cavity
ACCX12	N/A	<10%	20%	2	Trachea
ACCX14	N/A	<10%	90%	1	Trachea
ACCX15	N/A	100%	0	unk	Oral cavity
ACCX16	N/A	30%	80%	2	Bronchus
ACCX19	N/A	30%	60%	2	Oral cavity
ACCX20M1	N/A	30%	50%	1	Metastatic tumor to liver
ACCX2002	N/A	30%	50%	2	Parotid
ACCX21	N/A	30%	70%	1	Parotid
ACCX22	N/A	<10%	30%	1	Parotid

Tumor	MYB	ICN1	TP63	Grade	Tumor Site
ACCX24	N/A	<10%	0	2	
ACCX29	N/A	40%	80%	2	